JOURNAL OF APPLIED PHYSICS VOLUME 88, NUMBER 5 1 SEPTEMBER 2000

Atomistic simulation of diffuse x-ray scattering from defects in solids

K. Nordlund
Materials Research Laboratory, University of Illinois, Urbana, IL 61801, and Accelerator Laboratory, P.O. Box 43, FIN-00014 University of Helsinki, Finland

P. Partyka, R. S. Averback, and I. K. Robinson
Materials Research Laboratory, University of Illinois, Urbana, Illinois 61801

P. Ehrhart
Institut für Festkörperforschung, Forschungszentrum Jülich, Jülich, Germany

(Received 6 March 2000; accepted for publication 31 May 2000)

Diffuse x-ray scattering is a powerful means to study the structure of defects in crystalline solids. The traditional analysis of diffuse x-ray scattering experiments relies on analytical and numerical methods which are not well suited for studying complicated defect configurations. We present here an atomistic simulation method by which the diffuse x-ray scattering can be calculated for an arbitrary finite-sized defect in any material where reliable interatomic force models exist. We present results of the method for point defects, defect clusters and dislocations in semiconductors and metals, and show that surface effects on diffuse scattering, which might be important for the investigation of shallow implantation damage, will be negligible in most practical cases. We also compare the results with x-ray experiments on defects in semiconductors to demonstrate how the method can be used to understand complex damage configurations. © *2000 American Institute of Physics.* [S0021-8979(00)06017-5]

I. INTRODUCTION

Understanding the properties of point defects and dislocations is of great importance in many fields of technology. In semiconductor manufacturing the interactions of intrinsic defects and impurities play a crucial role in the doping of silicon.[1] In fission and fusion reactors, defects produced by neutrons determine the phase and dimensional stability as well as rate of wall material embrittlement.[2]

Diffuse x-ray scattering (DXS) is a useful tool for investigating point defects and defect clusters in solids.[3] The attractiveness of this technique derives from its ability to probe defects of sizes ranging from single point defects to rather large dislocation loops and to distinguish the type of defect, vacancy or interstitial. Much of what is now known about self-interstitials atoms in metals and the interactions of these defects, for example, has been gained through measurements of the Huang DXS, which refers to the scattering close to the Bragg peak.[3–5] The method is also subject of recent renewed interest due to the development of x-ray microbeams.[6] Despite the past success of this method, it has the drawback that it is often difficult to relate quantitatively measured scattering intensities to specific defects. The scattering must be calculated for a variety of possible defect configurations and then compared with experiments. These calculations require first determining the strain field around the defect and then evaluating the scattering from the equation,

$$S(\boldsymbol{K}) = \left| f_{\boldsymbol{K}} \sum_i e^{i\boldsymbol{K}\cdot\boldsymbol{R}_i} \right|^2, \tag{1}$$

where $\boldsymbol{K}$ is a reciprocal lattice vector and $\boldsymbol{R}_i$ the position of atom i in the crystal.[5]

For simple point defects and defect clusters, this equation can be performed analytically,[5,7] but for more complex defect structures, this is no longer possible and other methods are required. In the present investigation we provide a general framework for using computer simulations to evaluate the diffuse scattering from virtually any defect in most crystalline solids. The only requirement is that a suitable interatomic potential is available describing the solid of interest. Our present interest in this method concerns primarily defects in semiconductors that are produced by low-energy ion implantation.[8,1,9] For this situation, the computation of the scattering intensity is complicated by the presence of the surface and the correlations between the vacancy and interstitial defects.

The deceptively simple nature of Eq. (1) suggests an obvious approach to obtaining the DXS: simply create the atom positions $\boldsymbol{R}_i$ for a large number of atoms, and evaluate the sum directly. However, there are two main problems with this approach. The first is that a very large number of atoms (of the order of tens of millions or more) are typically needed to obtain convergence in the sum for the Huang scattering. The second is obtaining the displacement field.

The first attempts at directly evaluating the sum from atom positions were performed by Keating and Goland,[10] who showed that by modifying Eq. (1) with a convoluting exponential term,

$$S(\boldsymbol{K}) = \left| f_{\boldsymbol{K}} \sum_i e^{-\sigma^2 \boldsymbol{R}_i^2/2a^2} e^{i\boldsymbol{K}\cdot\boldsymbol{R}_i} \right|^2, \tag{2}$$

the convergence of the sum some distance from the Bragg peak can be speeded up significantly. In the convolution term

$\exp(-\sigma^2\boldsymbol{R}_i^2/2a^2)$ R_i is the distance to the defect center and a the lattice constant. The convolution factor σ has the effect of broadening the Bragg peak, but not affecting the DXS a distance proportional to σ/a in reciprocal space from the Bragg peak. Ehrhart *et al.* have used ''hybrid'' schemes where some, but not all, atom positions surrounding a defect have been used in the summation, combined with analytical averaging schemes to take care of the scattering contribution from missing atoms.[11] But because of its computational cost, and the fact that no good general methods for evaluating the atomic-level strain field existed, the direct summation method largely has fallen out of use.

Two recent developments, however, revive interest in the direct summation method. First, improvements in classical many-body interatomic potentials have made reliable calculations of strain possible in many materials, as these potentials can reproduce all first-order elastic constants and many defect properties.[12,13] Second, the vast increases in computer processor and memory capacity have made it possible to treat atomic interactions in systems consisting of millions of atoms.

Hence a combination of the old direct summation method (with greatly enhanced computational ability)with modern interatomic potentials for realistic simulations of possible defect structures opens up the possibility to calculate the x-ray scattering from even very complex atom configurations.

In this work, we present our fully atomistic direct summation method for calculating the DXS from defects in solids, and present simulation results for a wide range of defects in different configurations, with an emphasis on cases which are difficult or impossible to study with the classical analysis tools. Although some aspects of our simulation method have been discussed in preliminary form,[14–16] neither a complete presentation of the method and nor discussion of the simulation results has been presented before.

This article is organized as follows: In the next section, we present our two varieties of the simulation method. In Sec. III we present DXS simulation results for various defects configurations in the bulk, and in the following section we discuss how the presence of a surface affects the DXS from defects. Finally, in Sec. V we discuss some implications of our results for the analysis of DXS measurements.

II. SIMULATION METHOD

A. Large-sphere approach

We have used two approaches for calculating the DXS: a simple, brute-force, ''large-sphere'' approach, and an extrapolation method. These differ in the way the displacement field is obtained. The large-sphere method is presented in this subsection and the extrapolation method is summarized in the next. To make the presentation of the method concrete, we provide numerical examples from our studies on Si, Ge and FCC metals like Cu.

The basic idea of our methods is to obtain the coordinates of the displaced atoms surrounding a defect, and then directly evaluate Eq. (2). The number of atoms needed depends on many factors, but the most important is simply where in reciprocal space the scattering is of interest. For scattering between the Bragg peaks, it is possible to use a large value of σ (typically ~ 0.2), in which case the number of atoms can be kept small (of the order of one million). On the other hand, for Huang scattering, the value of σ must be reduced, and the number of atoms correspondingly increased. In the large-sphere approach we have included as many as 20 million atoms, while in the extrapolation method we have employed up to several hundreds of millions.

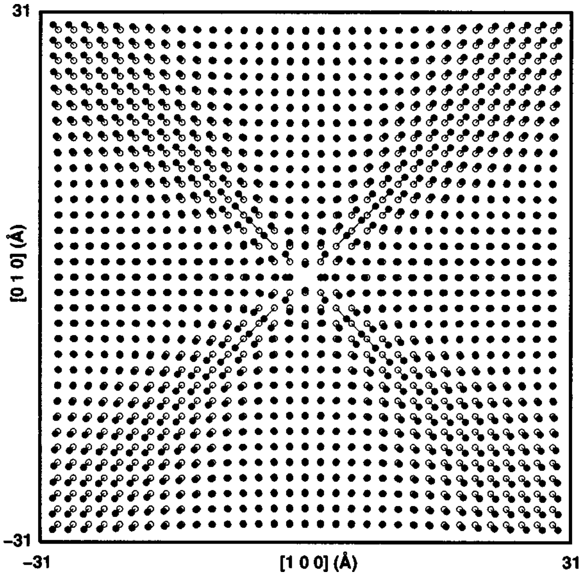

FIG. 1. Shape of strain field around a 100 dumbbell in Cu. The ''axis'' of the dumbbell was oriented along the [100] direction. The plots show the displacement in a 1 unit cell thick slice centered at the defect. The hollow circles denote the initial positions of the atoms, and the filled ones the final positions. The lines connect the initial and final position of each atom. To make the shape of the strain field better visible, the atom displacements were multiplied by a factor of $0.5r^2$, where r is the distance to the center of the defect. Note that some neighboring atoms lying along the [100] direction relax inwards.

Except for the surface calculations presented in Sec. IV, we normally surround the defect by a large sphere of atoms, with the center of the defect at the center of the sphere. This geometry introduces possible complications from relaxation or truncation at the outer surface of the sphere, but because of the term $\exp(-\sigma^2\boldsymbol{R}_i^2/2a^2)$ in Eq. (2), such surface effects become negligible and have not been a problem in our simulations.

The atomic displacements surrounding the defect, are obtained by minimizing the potential energy of the system using an appropriate classical interatomic force model. A typical resulting displacement field is illustrated in Fig. 1. Specifically, we have used the well-tested Stillinger–Weber[17] and Tersoff[18,19] interatomic force models for Si and Ge, and embedded-atom method (EAM) models for FCC metals.[20,12] A reassuring finding for the two models for Si and Ge is that despite their very different functional forms, and different physical properties used in fitting them,[13] they yield essentially the same scattering intensities. This behavior was found for a variety of defects in the two materials. All interatomic potentials used reproduce the elastic constants for cubic systems to within ~10%, and give reasonable surface properties.[13,12]

We note that the strain field far from the defect could also be calculated using finite element modeling (FEM). An atomistic approach would still be necessary close to the defect, however, and so a procedure to seamlessly combine the two method would be necessary. Although this is now possible,[21] nearly all problems of interest can be solved with the completely atomistic approach and we opted for this algorithmic simplicity in our calculations.

It was implied in the above that the displacement field of the defect derives directly from our classical interatomic potentials. The EAM models are known to describe a wide variety of defect properties in metals well,[12,22,23] and the direct procedure was, for them, indeed employed. In semiconductors, however, the charge state of a defect can play a large role in its structure,[24–26] and classical interatomic force models can in some cases fail miserably in describing even the structure of a defect. To deal with such cases, we use the atom coordinates obtained from an *ab initio* quantum mechanical simulation and fix the coordinates of the atoms which are part of or immediately adjacent to the defect, and thus incorporate them in the strain calculation. The classical potential is then employed for relaxation of atoms surrounding this region.

Once the potential energy minimum has been found (with the method described in Sec. II C below), the diffuse x-ray scattering is obtained by straightforward summation using Eq. (2). For comparison with experiment, the additional step of averaging the scattering intensities over all equivalent orientations of the defect in the lattice must be performed. In practice, the number of averaging directions can be substantially reduced by taking account of symmetries of the defect and scanning direction in reciprocal space.[27] For instance, in a scan along [100] in reciprocal space through a (400) Bragg peak, the reciprocal lattice vector $\boldsymbol{K}=(h,k,l)$ has only an h component, whence all permutations of atom coordinates involving only the y and z coordinates will be equivalent.

The large-sphere approach is mainly limited by available computer memory. The approach described in the next section greatly reduces the memory requirement.

B. Extrapolation approach

A far larger number of atoms can be employed in the calculation of the DXS by introducing an extrapolation procedure to obtain the atomic displacements far from the defect, and using the directly calculated displacements closer in. The two different regimes must then be smoothed to prevent artificial boundary effects. The calculation procedure is fairly complicated and involves several different atom cells. We summarize the central features of this method here; a detailed description can be found in Ref. 15.

The calculation starts with the defect in a small cubic defect cell. In the first stage of the calculation process, a spherical defect cell is created by surrounding the cubic cell atoms with atoms at perfect lattice positions out to a radius R_{SD}. This spherical shell is relaxed to its energy minimum using the relaxation procedure described below. Typically we use a sphere with a radius of the order of 100–150 Å.

Displacements of the atoms outside the spherical cell are obtained by assuming that they fall off as $1/\boldsymbol{R}_i^2$, a basic tenet of elasticity theory for bulk defects.[5] The angular distribution of the atom displacements is obtained by comparison with another spherical cell containing perfect atom positions and the same surface relaxation as the defect cell. This distribution is then used to obtain the displacements of atoms outside the radius R_{SD}. A lattice matching process[15] is used to ensure that the displacements are continuous at the interface at the radius R_{SD}.

The diffuse scattering is finally calculated using Eq. (2) using real atom coordinates inside R_{SD} and by creating extrapolated atom coordinates from the angular distribution outside this radius. Since the extrapolation approach needs to store the positions of only a few hundred thousands of atoms at a time, computer memory capacity is not a serious limitation. In principle the approach can be used to obtain the DXS scattering arbitrarily close to the Bragg peak, but since approaching the Bragg peak requires the (temporary) creation of ever greater number of atoms, the processor CPU speed becomes the limiting factor. We note, however, that the averaging scheme used by Ehrhart *et al.*[11] could be used to circumvent this limitation.

C. Atom relaxation

The problem of finding the strain field surrounding a defect essentially requires finding the closest local potential energy minimum of the system of atoms consisting of the defect atoms and its surroundings. To achieve this efficiently, we use either the conventional conjugate gradient (CG) method described in Ref. 28, or a modification of it. In the standard method, every iteration downward in potential energy first checks that a minimum exists in the direction of the atom's movement; it then uses a harmonic approximation of the potential energy hypersurface to move closer to this minimum. This approach requires about ten potential energy evaluations per iteration step.

In tests of the standard CG method for our systems of atoms we found that the line minimization step size,[28] λ, is almost equal throughout most of the iteration sequence. Furthermore, in the problem at hand it is very plausible that a minimum always exists in the next conjugate direction. Using these observations, we devised an ''adaptive conjugate gradient'' (ACG) method, in which the atoms are moved forward by an amount λ in the next conjugate direction, without any bracketing of the potential energy minimum. If this move leads to a decrease in potential energy, λ is slightly increased before the next step, and the process is repeated. If the move leads to an increase in potential energy, the atoms are moved back to their previous positions, λ is decreased by a factor of 2, and a new move is attempted. In the ACG method, only slightly more than 1 (typically 1.1–1.2) potential evaluations are on average needed per iteration step. On the other hand, since the ACG method does not follow the ''optimal'' path of conjugate directions,[28] ~3 times more iterations than in the CG method are typically needed. Thus the overall speedup is typically about a factor of 3.

Comparisons of the two relaxation schemes have shown that for defect configurations which are initially close to equilibrium, the two methods give essentially identical results. We note, however, that the ACG method may not be faster or even reliable in systems starting far from the local energy minimum. Since the changes in energy associated with the long-range strain fields are very small, we usually carry out the iterations to a precision of 10^{-10}–10^{-15} in the potential energy.

For the practical evaluation of the forces, we use a combined link-cell and neighbor-list to find the nearest neighbors of each atom efficiently.[29]

To obtain the relaxation volume[30] of defects, we embedded the defects in a cubic simulation cell with periodic boundaries, and used a molecular dynamics pressure relaxation scheme[31] to relax the cell to zero pressure, independently in each dimension. Comparison of the relaxed cell volume with that of a perfect simulation cell gives the relaxation volume.

III. DEFECTS IN THE BULK

In this section we present a few of our most important results for defects in the bulk, and in the discussion (Sec. V) we will demonstrate how they can be used to understand experimental results. We emphasize that as most of the defects treated here are described by classical potentials, their exact properties are not necessarily realistic in themselves. In particular, the configurations calculated for the small vacancy and interstitial clusters in Si have not been verified experimentally, however, they are still adequate for our purpose of examining how increasing defect size and relaxation volume affect the diffuse scattering line shapes.

In the following presentation of our simulation results, we do not distinguish between results obtained with the CG or ACG methods, or with the large-sphere or extrapolation scheme, as these have been found to give essentially identical results. Unless otherwise noted, the defect atoms have been described by the classical interatomic potential used for the strain field evaluation. All the results for defects in the bulk are averaged over all equivalent defect orientations. The scans shown are over (511), (400) or (220) Bragg peaks, since they are commonly used in experiments. Although the results for different Bragg peaks for a given defect do usually differ somewhat, the qualitative features and trends discussed here are usually independent of the choice of the peak.

A. FCC interstitial

The determination of the structure of the FCC interstitial is a major success of diffuse x-ray scattering, which was achieved in the early 1970s. The shape of the scattering arising from different interstitial configurations was predicted theoretically, and subsequent experiments showed that the interstitial has the split ⟨100⟩ dumbbell structure, at least in Al and Cu.[32,33]

As a test of our model, we calculated the DXS for the interstitial in Cu, since it is well described by our EAM models.[22] Figure 2 compares the resulting scattering pattern with the theoretical prediction of Dederichs[5] for a [400] reflection.[34] Figure 2 shows that the two calculations indeed agree very well; not only the dominating ''bow-tie'' shape along [100], but also the weak secondary maxima close to [010] are reproduced by our simulations. We also successfully reproduced the isointensity curves around the [110] and [111] reflections shown in Fig. 1 of Ref. 5.

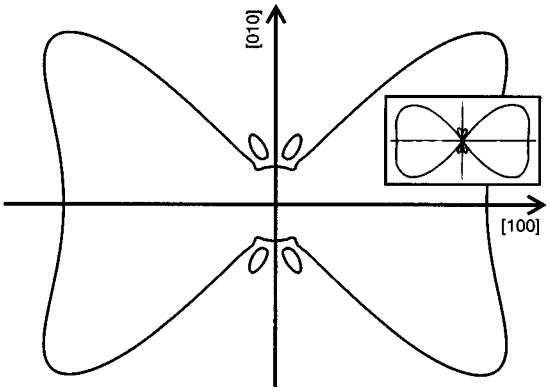

FIG. 2. Simulated iso-intensity curve of the symmetric (Huang) part of the diffuse scattering pattern for a dumbbell interstitial in Cu around the (400) Bragg peak. The inset shows the same scattering pattern predicted from analytical calculations (see Ref. 5) for an isotropic interstitial in Cu.

The small difference of the contours seen in the shapes in Fig. 2 is due to the fact that the theory used by Dederichs only includes nearest-neighbor forces, whereas the EAM model also includes interactions farther out. A calculation of the Kanzaki forces giving rise to the dipole tensor showed that the interactions farther than the nearest-neighbor shell contribute about 30% to the total interaction energy. Especially the role of the two second-nearest-neighbor atoms lying along the dumbbell [100] axis direction is interesting: these atoms actually relax slightly inwards (cf. Fig. 1) due to their interaction with the strongly upward-displaced nearest-neighbor atoms.

B. Single defects in Si and Ge

The structure and properties of small defects in semiconductors is of great current interest owing to their importance for ion implantation.[1] At present these properties are not well known. DXS methods could in principle be used to determine the structure of these defects. Some success has indeed been achieved at determining for instance the average distance between interstitials and vacancies in Frenkel pairs produced by electron irradiation,[35] and size estimates for interstitial and vacancy clusters,[6] but difficulties in predicting the scattering line shape in the diamond crystal structure have made it difficult to analyze more complex defects typical of ion implantation. We have calculated DXS line-shapes and spacemaps for a wide selection of defects in Si and Ge.

We first calculated the scattering from a single vacancy and dumbbell interstitial to check how well it conforms with the analytical prediction. In our Stillinger–Weber model, the vacancy and interstitial have relaxation volumes of −1.5 and +1.5 atomic volumes, respectively. These values are probably somewhat too large,[36] but as they are nearly equal in

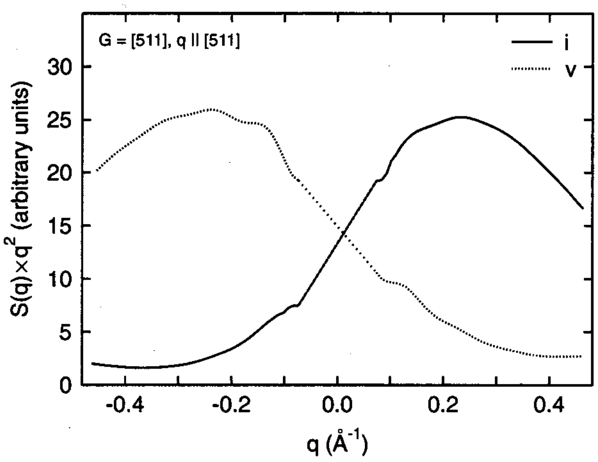

FIG. 3. Diffuse scattering of a vacancy (v) and $\langle 110 \rangle$ dumbbell interstitial (i) in Si. The scattering is plotted in units of Sq^2 vs q, where S is the scattering intensity and q the distance in reciprocal space to the Bragg peak G. The Bragg peak is left out of the figure, and the scattering lineshape of both defects interpolated in the middle to guide the eye.

absolute value the qualitative comparison of the vacancy and interstitial scattering is still relevant. The results are shown in Fig. 3 as a function of q, where q is the distance in reciprocal space to the Bragg peak **G**. We plot the results in units of Sq^2, which has proved to be a convenient way to see deviations from $1/q^2$ behavior. As expected[5] the vacancy has strong scattering at negative q, and the interstitial at positive q. We also verified that the symmetric part of the scattering, i.e., the average over the positive and negative sides, has an almost constant $1/q^2$ dependence close to the Bragg peak, as predicted for Huang scattering.[5,4]

Thus the results for a simple interstitial and vacancy conform to the classical theory. The use of atomistic simulations does have the advantage that it can also treat more complicated defect structures. Electron paramagnetic resonance (EPR) experiments and recent DFT calculations show that even the structure of the vacancy in Si and Ge can be quite complex for some charge states of the defect.[24–26,37] The atomistic simulations can be used to obtain the DXS from these defects by incorporating fixed DFT atom positions surrounding the defect into the simulations. To demonstrate that this method could, at least in principle, be used to determine the structure of vacancies in semiconductors we have calculated the DXS from different structures of the vacancy in Ge with different symmetries. The coordinates of the atoms surrounding the vacancy were obtained from DFT simulations.[37] The results are illustrated for three different symmetries of the defect in Fig. 4. It is clear that the symmetry of the scattering profile decreases with decreasing symmetry of the defect. The scattering of the tetrahedrally symmetric defect [Fig. 4(a)] has the familiar figure "8" shape expected for tetrahedrally symmetric defects.[3] The defects with lower-symmetry have quite different scattering patterns.

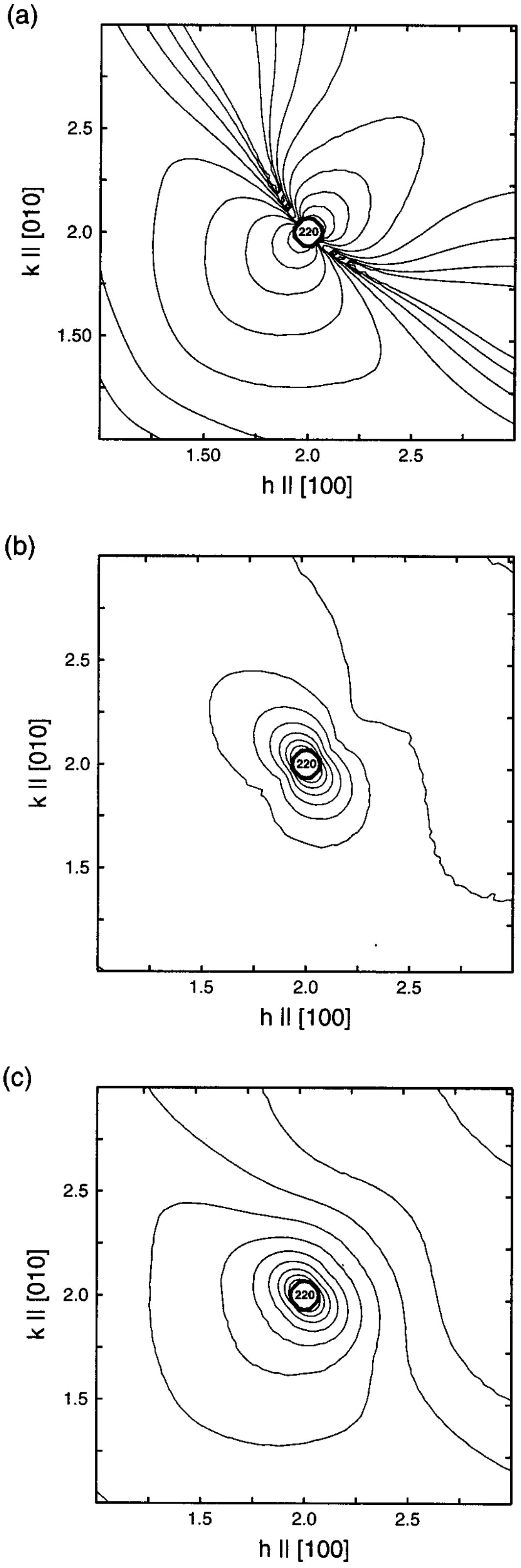

FIG. 4. Diffuse scattering iso-intensity curves around the (220) Bragg peak for three different vacancy structures in Ge. (a) shows the scattering for a vacancy with tetrahedral (T_d) symmetry, i.e., all four atoms surrounding the vacancy relaxing inwards toward it; (b) shows one with D_{2d} symmetry, i.e., two bonded atom pairs forming symmetrically on both sides of the vacancy; and (c) shows a lower-symmetry structure characteristic of negatively charged vacancies.

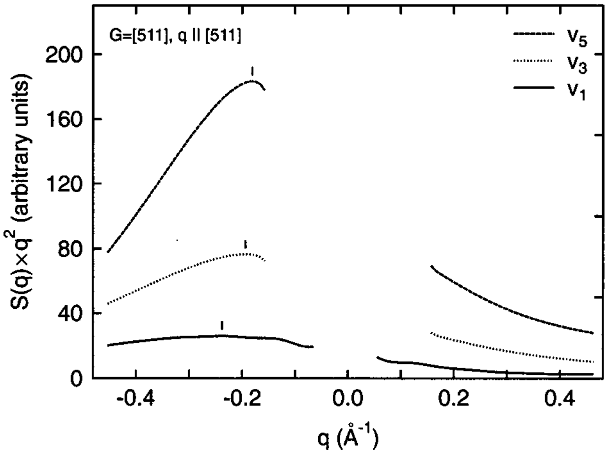

FIG. 5. Simulated diffuse scattering for three vacancy clusters v_j in Si, where j denotes the number of vacancies in the cluster. The Bragg peak has been left out of the figure. The locations of the maxima on the negative side are indicated by tiny vertical lines. The relaxation volumes of the mono-, tri- and pentavacancy used here are -1.5, -3.2 and -5.3 atomic volumes, respectively.

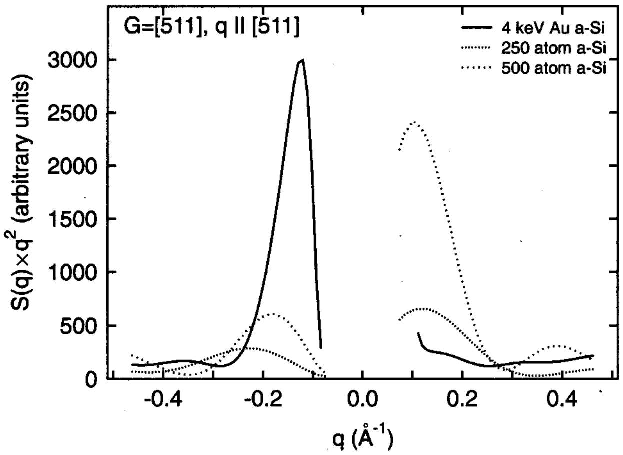

FIG. 7. Simulated diffuse scattering for a few amorphous clusters in Si. The ''4 keV Au *a*-Si'' indicates damage produced in a collision cascade induced by a 4 keV Au recoil in Si modeled by the Stillinger–Weber potential, and the two other labels amorphous Si with about 250 and 500 atoms with the experimental density of *a*-Si.

C. Defect clusters

The classical theory of x-ray scattering[5] predicts that the scattering intensity from defect clusters along radial scans will have a $1/q^2$ dependence close to the Bragg peak (Huang scattering), and a $1/q^4$ behavior far from it (Stokes–Wilson approximation). For small, very dense defect clusters in Cu we do observe this behavior, although the $1/q^4$ region is fairly narrow. For small clusters in Si, regions with well-defined q^{-2} and q^{-4} dependencies are not observed. The likely reason is that in the open crystal structure of Si it is difficult to create a dense defect with a large relaxation volume. By plotting the scattering intensities as Sq^2 plots, however, the size of the defect cluster can be obtained by locating the value of q where the scattering is a maximum, as now illustrated.

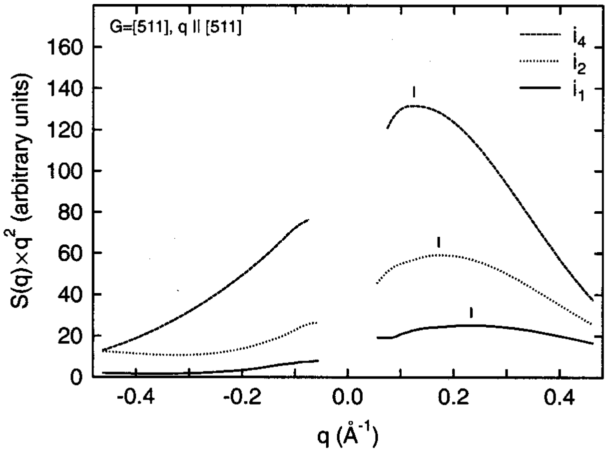

FIG. 6. Simulated diffuse scattering for three interstitials clusters i_j in Si, where j denotes the number of extra atoms in the cluster. The Bragg peak has been left out of the figure. The locations of the maxima on the positive side are indicated by tiny vertical lines. The relaxation volumes of the mono-, di- and tetrainterstitial used here are $+1.5$, $+2.6$ and $+4.3$ atomic volumes, respectively.

We calculated the DXS for a number of vacancy and interstitial clusters in Si. The defect configurations were created simply by adding or removing a few atoms in a small region of a crystal, and then relaxing the structure by a short molecular dynamics simulation at 300–600 K and subsequent quench to 0 K. DXS calculations of radial scans from vacancy clusters are shown in Fig. 5. We see that the scattering intensities from vacancy clusters are stronger on the negative side of the Bragg peak, as expected.[5] The locations of the maxima at negative q in this Sq^2 plot are proportional to the defect size; the larger the defect relaxation volume, the closer the maximum is to the Bragg peak located at $q=0$. Also, the decrease of the scattering beyond the maximum is more rapid for larger defects, corresponding to q exponents <-2, as predicted by theory for defect clusters.

The scattering from interstitial clusters is illustrated in Fig. 6. The shape of the scattering is qualitatively a mirror image of that for vacancy clusters. The scattering is stronger on the positive side, and the maxima shift toward the Bragg peak with increasing defect size. Similar behavior was seen for larger interstitial and vacancy clusters as well, up to clusters containing 64 defects (with relaxation volumes of roughly 50 atomic volumes). The integrated diffuse scattering was proportional to the square of the relaxation volume of the defect, as expected.[5]

Other defect agglomerates, such as amorphous zones and damage produced by collision cascades, exhibited similar behavior. Damage with a positive or negative relaxation volumes had stronger scattering at positive or negative q, respectively. Large amorphous zones produced sharp and distinct peaks in the scattering close to the Bragg peak. Some results are illustrated in Fig. 7. The ''4 keV Au'' is the damage produced by a 4 keV Au recoil in Si. The defect zone, which appears to be amorphous, contains about 900 atoms and has a relaxation volume of $-30\ \Omega$, where Ω is the atomic volume. Whether the Stillinger–Weber (S-W) potential describes Si amorphized by implantation adequately is questionable, since it has been reported that amorphous Si is

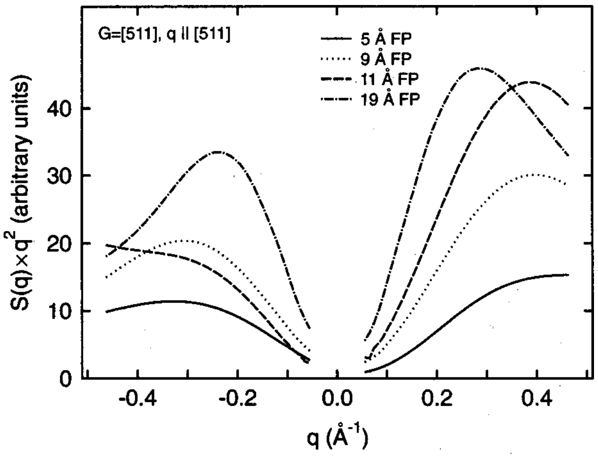

FIG. 8. Simulated diffuse scattering for four Frenkel pairs in Si. The Frenkel pairs are labeled with the separation between the interstitial and vacancy that form the pair. The relaxation volumes of all pairs are close to zero.

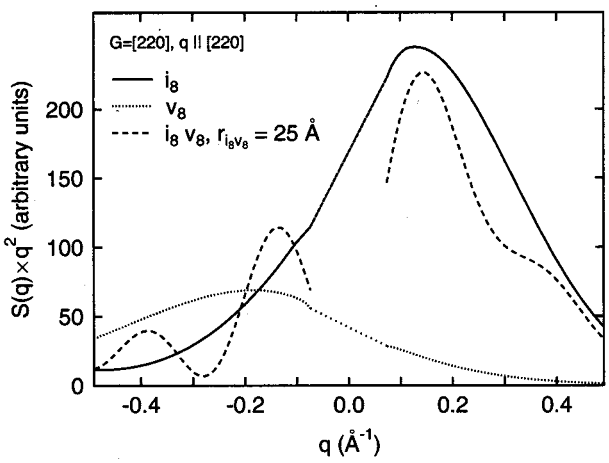

FIG. 9. Diffuse scattering of an octa-vacancy (v_8) and octa-interstitial (i_8) in Si, and a defect consisting of both the v_8 and i_8 separated by 25 Å. The Bragg peak is left out of the figure, and the scattering lineshape of the single clusters interpolated in the middle to guide the eye. The relaxation volumes of the i_8, v_8 and combined $i_8\, v_8$ defects used here are +8.0, −4.0 and +4.0 atomic volumes, respectively.

slightly less dense than crystalline Si,[38] whereas the S-W potential predicts a slightly larger density. To account for the possible error in the density, we also created *a*-Si spheres with relaxation volumes corresponding to the experimental density (1.8% less than that of *c*-Si[38]) simply by adding a few atoms into the *a*-Si zone. The *a*-Si spheres where relaxed with a short constant-temperature simulation before the DXS calculations. For the spheres shown in Fig. 7 the 250 atom *a*-Si zone has a relaxation volume of +5.1 Ω and the 500 atom cluster one of +10.7 Ω. This shows that amorphous Si inclusions produced, e.g., by ion or neutron irradiation can be expected to produce a large DXS signal, unless the strain surrounding them is otherwise relieved.

D. Defect pairs and correlation effects

The most common way of introducing defects into solids is by electron and ion irradiation, which usually produce Frenkel pairs as the initial state of damage. Hence understanding the DXS line shape from Frenkel pairs is also of great interest. We have calculated the scattering from several Frenkel pairs in Si with different separations between the interstitial and vacancy. The Stillinger–Weber interatomic potential gives about the correct structure for both the [110] dumbbell interstitial[39,40] and the tetrahedral vacancy in Si. Most importantly, it gives relaxation volumes for these two defects which, in agreement with experiments, cancel almost exactly,[41,42] making it well suited for this study.

The results are shown in Fig. 8. The pairs are listed as a function of the separation between the interstitial and vacancy forming the pair. The scattering decreases close to the Bragg peak due to the cancellation of relaxation volumes and correlation effects between the interstitial and vacancy.[36]

Analysis of the data shows that the separation between the peaks on the negative and positive side is inversely proportional to the distance between the vacancy and interstitial — the defect with a separation of 19 Å has both peaks close to the Bragg peak, whereas one of the peaks of the 5 Å pair extends outside the figure. Furthermore, comparison of the scattering calculated for different Bragg peaks showed that the separation between the peaks is about the same in units of *q*. This enables a determination of the average separation between the vacancy and interstitial that form the pair, as suggested by Ehrhart, who used a simple superposition model of spherical defects to obtain the displacement fields.[36] The advantage of using an atomistic scheme is that as interatomic potentials and quantum mechanical force models are developed further, they can be expected to give increasingly accurate and detailed results.

To further illustrate the correlation effects, we calculated the DXS from an eight-interstitial and eight-vacancy cluster both separately and after placing the two defects in the same simulation cell, separated by 25 Å. The result is shown in Fig. 9. The single defect clusters have maxima either on the positive or negative side of the Bragg peak, as expected from Sec. III C, and a smooth behavior at the Bragg peak. For the combined cluster, however, the scattering pattern decreases close to the Bragg peak at both positive and negative *q*, again illustrating the correlation effects.

E. Dislocation loops

The scattering expected from perfect and partial dislocation loops in FCC metals is relatively well understood due to the calculations of Ehrhart, Trinkaus and Larson.[11] Since the diamond lattice can be viewed as two interpenetrating FCC lattices, and the dislocation properties in the two lattice types are in many respects similar,[43] it may seem reasonable to assume that the DXS from dislocations in Si would be similar to that in FCC metals. On the other hand, there are obvious differences between the materials, the most important of which is the nature of the covalent bonding in Si, leading to a more open crystal structure.

To test whether it is reasonable to assume a similarity between the diamond and FCC structures, we have simulated the DXS from extrinsic stacking faults in Si. In FCC metals, the scattering pattern from a bound extrinsic stacking fault has a very distinct shape, with scattering ''streaks'' in recip-

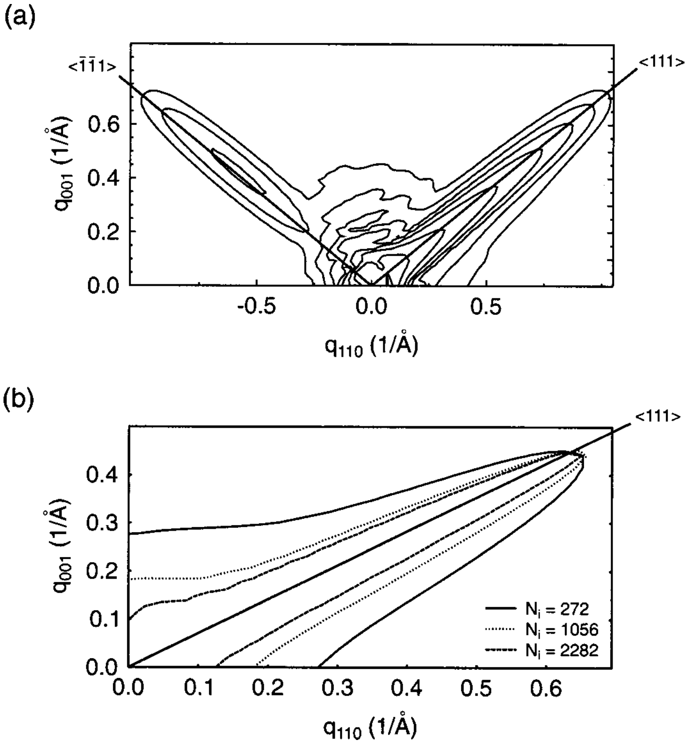

FIG. 10. Simulated DXS pattern from a stacking fault formed by about 1000 interstitial atoms in Si. (a) Scattering on the positive q_{001} side of the Bragg peak. q_{110} indicates the distance from the (220) Bragg peak in reciprocal space along the 110 direction and q_{001} in the vertical 001 direction. (b) Shape of the ⟨111⟩ streak emanating from the (220) peak for three stacking faults with different numbers of interstitial atoms N_i. The iso-intensity curves have been chosen so that their maxima along ⟨111⟩ coincide.

rocal space extending all the way from one Bragg peak to another.[11] Our result is shown in Fig. 10 for the scattering around the (220) Bragg peak. The scattering streaks are very similar to those in FCC metals, showing that at least in this case the x-ray scattering is similar in the two crystal structures. The location of the nodal minima in the scattering, however, are not the same as for the FCC stacking faults.

The advantage of using the atomistic simulation to study DXS from loops is that it is straightforward to study size effects, such as, for instance, determining at what size a stacking fault gives rise to a streak pattern. The inset in Fig. 10 shows how the streak pattern emerges as the size of the stacking fault grows. The streak pattern becomes visible for stacking faults with between 100 and 200 atoms in the stacking fault (double) plane.[43] Additional details of these simulations, and a comparison with experiments, will be given elsewhere.[44]

We also calculated the scattering pattern of a stacking fault tetrahedron (SFT) in Cu, i.e., a perfect tetrahedron formed by four triangular vacancy-type stacking fault loops lying on intersecting {111} crystal planes.[43,45] These defects are of great interest for understanding fission and fusion reactor wall material embrittlement by neutrons produced in the reactor.[45,46,2] Due to their nature of several intersecting stacking fault planes, and since the SFTs formed during irradiation are commonly only a few nm in size, calculating the DXS lineshape from an SFT could be quite difficult with analytical methods. On the other hand, we have recently found that the Cu EAM models give a good description of SFTs.[23]

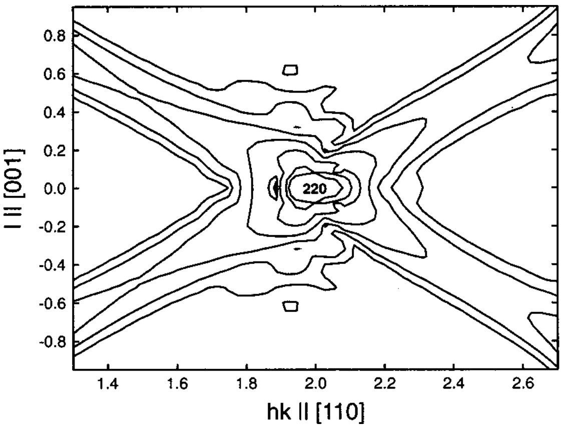

FIG. 11. X-ray scattering pattern from a stacking fault tetrahedron in Cu, in the plane spanned by the [110] and [001] crystal directions. The scattering in the streaks starts to increase at the outer edges of the figure because they start to approach other Bragg peaks.

Our result for the x-ray iso-intensity contours for an SFT with a side length of 10 nearest-neighbor distances (containing 55 vacancies) is shown in Fig. 11. Overall, the streak shape of the scattering resembles that from stacking faults (see Fig. 10 and Ref. 11). There are differences, however. Because of the vacancylike nature of the SFT, no points of vanishing intensity are observed.[11] Also since the SFT is a vacancylike defect, the scattering intensity is somewhat stronger on the negative [110] side of the Bragg peak.

IV. DEFECTS CLOSE TO A SURFACE

When a defect is close to a surface, the strain field deviates from the characteristic $1/r^2$ dependence. Barabash and Krivoglaz have derived general expressions for the DXS from defects in the vicinity of surfaces.[47] They concluded that the DXS from defects close to the surface will be close to the bulk value if $D_e \gg 1/q$, where D_e is the effective depth of the defects. For a value of $q \sim 0.1$ Å^{-1} this would mean that only defects very close ($\sim$10 Å) to the surface would have a DXS significantly differing from the bulk value. Although the Krivoglaz model thus gives a useful guideline for estimating when surface effects may be important, its mathematical complexity makes it difficult to obtain a more accurate estimate for real defects. The model also showed that surface effects can be even more prominent in thin films, which was later confirmed by experiment,[48] but this case is not of concern here. On the other hand, Grotehans *et al.* have shown that surface effects may affect the scattering at least very close to the Bragg peak.[49]

We simulated surfaces by simply replacing the sphere in the ''large-sphere approach'' by a hemisphere, placing the defect at some depth *d* below the (001) surface of the hemisphere. Because the presence of the surface breaks some of the symmetry in the scattering problem, a comparison with experiments requires a different averaging scheme than the

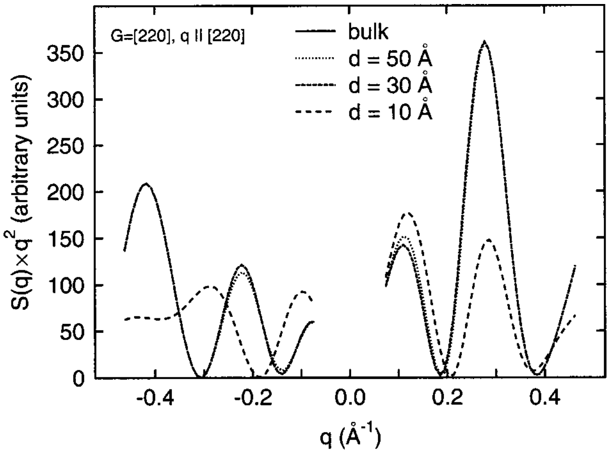

FIG. 12. Diffuse x-ray scattering for an in-plane peak for the damage produced by a 2 keV recoil in Si placed at different depths in the simulation cell. At the depth of 10 Å the surface intersects the damage region, and a small part of the damage is in fact cut off at the surface. It is noteworthy that even at 30 Å, when the damaged region is very close to the surface, the DXS is only slightly modified from the bulk value.

bulk calculations. Otherwise the surface DXS simulation method is identical to the approach presented in Sec. II A.

We first calculated the DXS for scattering directions parallel to the surface (''in-plane'' peaks). We simulated small vacancy clusters and cascade damage (with 2–20 defects), and compared the results to the bulk scattering for the same defects. For clusters containing 2–20 vacancies 50 Å below the surface, the DXS showed no effects of the surface within the numerical accuracy of the calculation. Figure 12 shows the scattering as a function of depth for the total damage produced in a 2 keV cascade (created in a typical collision cascade simulation[50]). The cascade contains 16 Frenkel pairs, some of them in clusters. This damage had a total relaxation volume of -1.4Ω. Due to the complex nature of the damage, the scattering line shape is quite complex, making this event a sensitive test for possible surface effects. This damage can be considered a rough representation of typical ion beam damage for nonoverlapping cascades, although in a real experiment the DXS result would of course be averaged over a large number of damage regions.

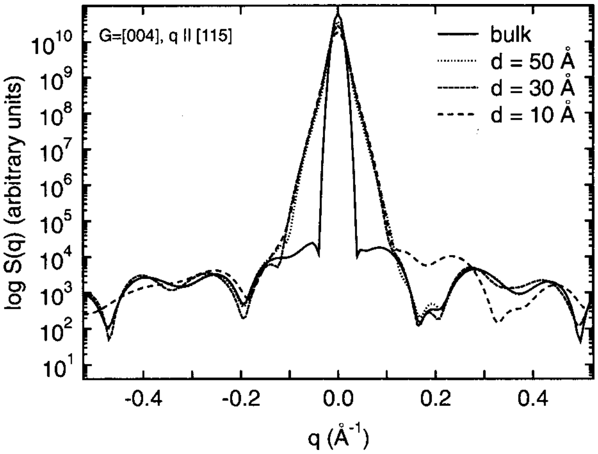

FIG. 13. Diffuse x-ray scattering for an out-of-plane [004] peak and a close-to-normal [115] scanning direction for the damage produced by a 2 keV recoil in Si placed at different depths in the simulation cell. Note that all the surface calculations have a broadened Bragg peak due to the scattering contribution from the crystal truncation rod. The diffuse scattering outside the truncation rod region is again similar to the bulk value except when the damage depth $\lesssim 30$ Å.

It is well-known that a diffraction vector perpendicular to a surface will exhibit a large diffraction streak, called a crystal truncation rod[51] due to the truncation of the crystal at the surface. Hence it is not useful to attempt to study the DXS in scattering directions exactly normal to the surface, as any diffuse contribution would be overshadowed by the truncation rod. It is, however, possible to study the DXS in a direction slightly tilted off the normal direction. In such a direction the Bragg peak will be somewhat broadened due to the truncation rod, but outside the broadened region the diffuse scattering will not be affected by the truncation effect. The results for one such simulation are illustrated for the 2 keV damage in Fig. 13.

For all depths greater than 30 Å the surface effects are negligible, both for the in-plane and out-of-plane peaks. In the out-of-plane peaks some effects of the surface start to be visible for a depth of 30 Å, but the overall shape of the DXS is still similar to the bulk result. We also did simulations of iso-intensity curves in the planes spanned by [110] and [001] and [100] and [001] crystal directions for the 2 keV damage at different depths but even in these much larger regions of reciprocal space the results were almost identical for depths greater than 30 Å.

At the depth of 10 Å the surface strongly affects the shape of the scattering. The extension of the central damage region in the cascade defect distribution is roughly 30 Å in each dimension, however, so at this depth the damage in the cell already intersects the surface. For most practical ways of introducing defects into materials (such as ion implantation, impurity diffusion and growth) the damaged region is usually at least some hundreds of Angstroms thick. Consequently the small surface effect found for the defects closest to the surface will rarely be of significance. Moreover, even in grazing incidence x-ray experiments, where the angle of incidence is less than the critical angle for total external reflection, the evanescent waves penetrate a few hundred Angstroms.

From the present simulations we cannot rule out that there is a larger surface contribution closer to the Bragg peak than what we can simulate now (such as the regime $qa/2\pi \lesssim 0.03$ considered by Grotehans *et al.*[49]). However, the range we have been able to simulate so far ($qa/2\pi \gtrsim 0.05$) is usually also the one studied in experiments.

V. DISCUSSION

One of the major differences of our results for defects in semiconductors compared to most experiments and models in metals is that the q dependence is weaker than q^{-2} close to the Bragg peak. In the Sq^2 plots this is clearly visible as a *decrease* of Sq^2 close to the Bragg peak. As pointed out by Ehrhart, the deviation from a q^{-2} dependence arises from the correlation in the distances between the vacancy and interstitial in a close Frenkel pair. In most metals, however, the

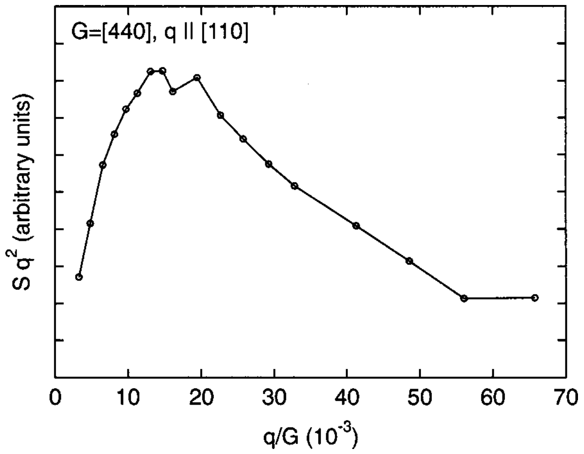

FIG. 14. Symmetric part of the diffuse x-ray scattering in neutron-irradiated Si. Data are taken from Fig. 4 in Ref. 42, and replotted as an Sq^2 plot.

relaxation volume of the interstitial is nearly ten times larger than that of the vacancy, and the correlation does not give rise to a cancellation in the long-range strain field of the interstitial. In semiconductors, the relaxation volumes of vacancies and interstitials are comparable, giving rise to correlation effects.

The importance of the correlation effect has not been fully realized in many x-ray studies of defects in Si. For instance, Mayer and Peisl reported a deviation from q^{-2} behavior in neutron-irradiated Si,[42] attributing it to resolution effects in the points closest to the Bragg peak. Replotting the data as Sq^2, however, shows that the deviation from q^{-2} behavior occurs over a fairly wide q range (see Fig. 14), with the maximum occurring at $q = 0.1$ Å^{-1}. Comparison with Figs. 9, 6 and 7 shows that this damage resembles that of cascade damage containing nearby interstitial- and vacancy-like point defects or defect clusters. Hence we believe it is very likely that the decrease close to the Bragg peak arises from a correlation effect.

Figure 15 shows the DXS in 20 keV Ga implanted Si for different doses below the amorphization threshold. As in the neutron damage, the maximum in the Sq^2 plot occurs at q ~ 0.1 Å^{-1}, characteristic for cascade damage. At high doses, the scattering is much stronger on the positive side, indicating that the type of damage dominating the DXS is interstitial clusters, or other defects with a large positive relaxation volumes (cf. Figs. 6 and 9). Details of these experiments will be published elsewhere.[52]

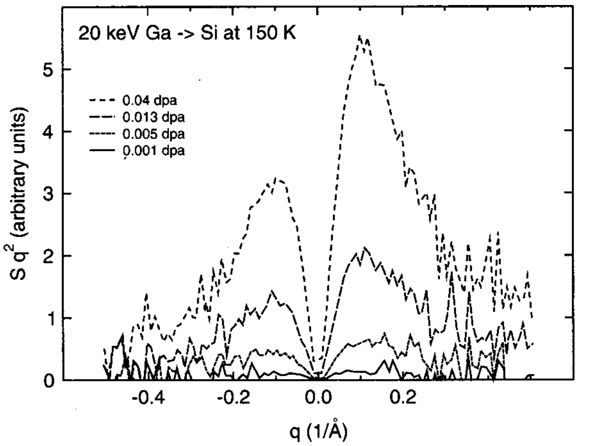

FIG. 15. Radial scan of diffuse scattering from Ga-implanted Si at 150 K for different doses (given in units of displacements per atom). From Refs. 52 and 53.

VI. CONCLUSIONS

We have described herein a fully atomistic method for analyzing diffuse x-ray scattering. The method is based on using modern interatomic force models and efficient atomistic simulation algorithms to obtain the strain field surrounding the defect. From the positions of the displaced atoms the x-ray scattering is then obtained by direct summation. Compared to analytical and numerical tools for analyzing DXS measurements, our method has the advantage that the same formalism can be used for a wide range of defects. We first compared the results of our method to those of analytical calculations for well-understood test cases to demonstrate that the method works reliably. We then used the method to evaluate x-ray lineshapes for technologically interesting defects which are difficult to treat by traditional means, such as stacking fault tetrahedra in metals and small defect clusters and stacking faults in Si. We also showed the effect of a nearby surface on the DXS from defects in a semi-infinite crystal is negligible except when the damaged region starts to intersect with the surface, or possibly very close to the Bragg peak. Finally, by comparison with experiments we have demonstrated how the calculations can be helpful for understanding defect properties in semiconductors.

ACKNOWLEDGMENTS

We acknowledge Dr. T. H. Metzger and Dr. U. Beck for useful discussions, and thank Dr. M. Tang, Dr. T. Diaz de la Rubia, J. Lento, Dr. J.-L. Mozos and Professor R. Nieminen for providing DFT atom coordinates of defects in semiconductors. The research was supported by the US Department of Energy, Basic Energy Sciences under Grant No. DEFG02-91ER45439, and by the Academy of Finland under Project Nos. 45481 and 44215. Grants of computer time from the Center for Scientific Computing in Espoo, Finland, the National Computational Science Alliance in Champaign, IL, and the National Energy Research Computer Center at Berkeley, CA are gratefully acknowledged.

[1] E. Chason, S. T. Picraux, M. Poate, J. O. Borland, M. I. Current, T. Diaz de la Rubia, D. J. Eaglesham, O. W. Holland, M. E. Law, C. W. Magee, J. W. Mayer, J. Melngailis, and A. F. Tasch, J. Appl. Phys. **81**, 6513 (1997).
[2] S. J. Zinkle, Radiat. Eff. Defects Solids **148**, 447 (1999).
[3] P. Ehrhart, J. Nucl. Mater. **216**, 170 (1994).
[4] K. Huang, Proc. R. Soc. London, Ser. A **190**, 102 (1947).
[5] P. H. Dederichs, J. Phys. F: Met. Phys. **3**, 471 (1973).
[6] M. Yoon, B. C. Larson, J. Z. Tischler, T. E. Haynes, J.-S. Chung, G. E. Ice, and P. Zschack, Appl. Phys. Lett. **75**, 2791 (1999).
[7] H. Trinkaus, Z. Naturforsch. A **28**, 980 (1973).
[8] L. Pelaz, M. Jaraiz, H. H. Gilmer, H.-J. Gossman, C. S. Rafferty, D. J. Eaglesham, and J. M. Poate, Appl. Phys. Lett. **70**, 2285 (1997).
[9] D. F. Downey, C. M. Osburn, and S. D. Marcus, Solid State Technol. **40**, 71 (1997).

[10] D. T. Keating and A. N. Goland, Acta Crystallogr., Sect. A: Cryst. Phys., Diffr., Theor. Gen. Crystallogr. **27**, 134 (1971).

[11] P. Ehrhart, H. Trinkaus, and B. C. Larson, Phys. Rev. B **25**, 834 (1982).

[12] M. S. Daw, S. M. Foiles, and M. I. Baskes, Mater. Sci. Rep. **9**, 251 (1993).

[13] H. Balamane, T. Halicioglu, and W. A. Tiller, Phys. Rev. B **46**, 2250 (1992).

[14] P. J. Partyka, R. S. Averback, K. Nordlund, I. K. Robinson, D. Walko, P. Ehrhart, T. Diaz de la Rubia, and M. Tang, in *Microstructure Evolution During Irradiation*, Vol. 439 of *MRS Symp. Proc.*, edited by I. M. Robertson, G. S. Was, L. W. Hobbs, and T. Diaz de la Rubia (Materials Research Society, Pittsburgh, 1997), pp. 89–94; the same paper is also published in *MRS Symp. Proc.* Vol. 438, p. 77.

[15] K. Nordlund, P. Partyka, and R. S. Averback, in *Defects and Diffusion in Silicon Processing*, Vol. 469 of *MRS Symposium Proceedings*, edited by T. Diaz de la Rubia, S. Coffa, P. A. Stolk, and C. S. Rafferty (Materials Research Society, Pittsburgh, 1997), pp. 199–204.

[16] K. Nordlund, P. Partyka, Y. Zhong, I. K. Robinson, R. S. Averback, and P. Ehrhart, Nucl. Instrum. Methods Phys. Res. B **147**, 399 (1999).

[17] F. H. Stillinger and T. A. Weber, Phys. Rev. B **31**, 5262 (1985).

[18] J. Tersoff, Phys. Rev. B **38**, 9902 (1988).

[19] J. Tersoff, Phys. Rev. B **39**, 5566 (1989); *idem* **41**, 3248 (1990).

[20] S. M. Foiles, Phys. Rev. B **32**, 3409 (1985).

[21] E. B. Tadmor, M. Ortiz, and R. Phillips, Philos. Mag. A **73**, 1529 (1996).

[22] K. Nordlund and R. S. Averback, Phys. Rev. Lett. **80**, 4201 (1998).

[23] K. Nordlund and F. Gao, Appl. Phys. Lett. **74**, 2720 (1999).

[24] J. W. Corbett, J. Nucl. Mater. **108 & 109**, 617 (1982).

[25] G. D. Watkins, in *Defects and Diffusion in Silicon Processing*, Vol. 469 of *MRS Symposium Proceedings*, edited by T. Diaz de la Rubia, S. Coffa, P. A. Stolk, and C. S. Rafferty (Materials Research Society, Pittsburgh, 1997), p. 139.

[26] M. J. Puska, S. Pöykkö, M. Pesola, and R. M. Nieminen, Phys. Rev. B **58**, 1318 (1998).

[27] H. Trinkaus, Phys. Status Solidi B **51**, 307 (1972).

[28] W. H. Press, S. A. Teukolsky, W. T. Vetterling, and B. P. Flannery, *Numerical Recipes in C; The Art of Scientific Computing*, 2nd ed. (Cambridge University Press, New York, 1995).

[29] M. P. Allen and D. J. Tildesley, *Computer Simulation of Liquids* (Oxford University Press, Oxford, England, 1989).

[30] P. Ehrhart, in *Properties and Interactions of Atomic Defects in Metals and Alloys*, Vol. 25 of *Landolt-Börnstein, New Series III*, edited by H. Ullmaier (Springer, Berlin, 1991), Chap. 2, p. 88.

[31] H. J. C. Berendsen, J. P. M. Postma, W. F. van Gunsteren, A. DiNola, and J. R. Haak, J. Chem. Phys. **81**, 3684 (1984).

[32] P. Ehrhart, H.-G. Haubold, and W. Schilling, Adv. Solid State Phys. **14**, 87 (1974).

[33] H.-G. Haubold, J. Appl. Crystallogr. **8**, 175 (1975).

[34] We note that Dederichs's calculation is for an isotropic point defect with all dipole tensor elements P_{ii} equal. But since the tetragonal deviation $|P_{11}-P_{22}|$ is experimentally known to be very small for the dumbbell structure (see Ref. 32), this comparison is relevant for our purpose. We also checked that the tetragonal deviation is small for the interstitial in our model.

[35] H. Zillgen and P. Ehrhart, Nucl. Instrum. Methods Phys. Res. B **127-128**, 27 (1996).

[36] P. Ehrhart and H. Zillgen, in *Defects and Diffusion in Silicon Processing*, Vol. 469 of *MRS Symposium Proceedings*, edited by T. Diaz de la Rubia, S. Coffa, P. A. Stolk, and C. S. Rafferty (Materials Research Society, Pittsburgh, 1997), p. 175.

[37] J. Lento, J.-L. Mozos, M. Puska, and R. M. Nieminen (unpublished).

[38] J. S. Custer, M. O. Thompson, D. C. Jacobson, J. M. Poate, S. Roorda, W. C. Sinke, and F. Spaepen, Appl. Phys. Lett. **64**, 437 (1994).

[39] R. Car, P. Blochl, and E. Samrgiassi, Mater. Sci. Forum **83-87**, 433 (1992).

[40] M. Tang, L. Colombo, J. Zhu, and T. Diaz de la Rubia, Phys. Rev. B **55**, 14279 (1997).

[41] A. R. Chelyadinskii, Sov. Phys. Solid State **18**, 506 (1976).

[42] W. Mayer and H. Peisl, J. Nucl. Mater. **108 & 109**, 627 (1982).

[43] J. P. Hirth and J. Lothe, *Theory of Dislocations*, 2nd ed. (Krieger, Malabar, FL, 1992).

[44] K. Nordlund, U. Beck, T. H. Metzger, and J. R. Patel, Appl. Phys. Lett. **76**, 846 (2000).

[45] B. L. Eyre, J. Phys. F: Met. Phys. **3**, 422 (1973).

[46] M. Kiritani, T. Yoshiie, and S. Kojima, J. Nucl. Mater. **141-143**, 625 (1986).

[47] R. I. Barabash and M. A. Krivoglaz, Fiz. Tverd. Tela (Leningrad) **29**, 3081 (1987); Sov. Phys. Solid State **29**, 1768 (1987).

[48] D. Bahr, W. Press, R. Jebasinski, and S. Mantl, Phys. Rev. B **51**, 12223 (1995).

[49] S. Grotehans, G. Wallner, E. Burkel, H. Metzger, J. Peisl, and H. Wagner, Phys. Rev. B **39**, 8450 (1989).

[50] K. Nordlund, M. Ghaly, R. S. Averback, M. Caturla, T. Diaz de la Rubia, and J. Tarus, Phys. Rev. B **57**, 7556 (1998).

[51] I. K. Robinson and D. J. Tweet, Rep. Math. Phys. **55**, 599 (1992).

[52] P. J. Partyka, K. Nordlund, I. K. Robinson, R. S. Averback, and P. Ehrhart (unpublished).

[53] P. J. Partyka, Ph. D. Thesis, University of Illinois at Urbana-Champaign, Urbana, IL 61801 (1997).